J. Fluid Mech. (1986), *vol.* 168, *pp.* 337–367
Printed in Great Britain

The nonlinear instability of Hill's vortex

By C. POZRIKIDIS†

Department of Chemical Engineering, University of Illinois, 1209 W. California St., Box C-3, Urbana, IL 61801, USA

(Received 11 July 1985 and in revised form 10 December 1985)

The nonlinear instability of Hill's spherical vortex, subject to axisymmetric perturbations is considered. The problem is formulated as a nonlinear integrodifferential equation for the motion of the vortex boundary. This equation is solved employing a numerical procedure which involves a piecewise representation of the vortex contour with discrete elements. This formulation offers an efficient method for studying a variety of vortex flows in axisymmetric geometry.

Our results indicate that if Hill's vortex becomes a prolate spheroid, a certain amount of rotational fluid is detrained from the rear stagnation point of the vortex, leaving behind a reduced vortex of approximately spherical shape. The amount of detrained fluid is a function of the initial deformation. If the vortex becomes an oblate spheroid, irrotational fluid is entrained into the vortex from the rear stagnation point, reaches the front vortex boundary, and circulates along the vortex boundary in a spiral pattern. In this fashion, the vortex reduces to a nearly steady vortex ring whose asymptotic structure is a function of the initial deformation. The structure of the asymptotic rings arising from oblate vortices is similar to that of steady rings described by Norbury (1973). The vortex speed is shown to tend to a constant value for prolate perturbations, and to fluctuate around a mean value for oblate perturbations.

1. Introduction

A variety of flows at high Reynolds number are characterized by axisymmetric regions of fluid with concentrated vorticity. Examples include jets, atmospheric plumes and wakes behind axisymmetric bodies. The dynamics of these flows involves complex phenomena, such as formation and interaction of axisymmetric coherent vortices, whose nature is not well understood. Most of the available information comes from experimental studies using velocity measurements and/or flow visualization, while only a few analytical studies have been attempted.

A fundamental understanding of the above flows may be accomplished by analysing appropriate simple configurations, amenable to analytical or numerical methods (O'Brien 1961; Norbury 1973; Durst & Schönung 1982). Hill's spherical vortex provides a convenient prototype for this purpose (Hill 1894). This vortex arises in applications including the motion of bubbles and droplets at high Reynolds number (Moore 1962; Harper & Moore 1968), the formation of laminar wakes behind spherical cap bubbles (Wegener & Parlange 1973) and the rise of thermals due to natural convection (Turner 1964).

From a mathematical point of view, Hill's vortex constitutes an extreme member

† Present address: Research Laboratories, Eastman Kodak Company, Rochester, NY 14650, USA.

of a family of steady axisymmetric vortices translating in infinite irrotational fluid (Norbury 1973). As a common characteristic, the vorticity inside these vortices is a linear function of the distance from the axis of symmetry. The members of this family range from Hill's vortex, to vortex rings of very small cross-section.

Concentrating on Hill's vortex, we study the evolution of axisymmetric perturbations that make the vortex a spheroid. These perturbations may be introduced by local straining flow fields; examples include droplets falling in converging geometries or approaching solid boundaries. Moffatt & Moore (1978) studied the initial evolution for small deformations by linearizing the governing equations. They showed that when the vortex becomes an oblate spheroid, irrotational fluid is entrained into the vortex from the rear stagnation point, and the vortex reduces to a vortex ring. On the other hand, when the vortex becomes a prolate spheroid, rotational fluid is detrained from the vortex in the form of a spike, growing from the rear stagnation point; in physical terms, the disturbance is swept away by the outer flow, leaving behind a vortex of reduced radius.

The restrictions of linear theory make the above results strictly valid only for disturbances of very small initial amplitude and for limited evolution time. It is of interest to extend the analysis to include finite initial amplitudes, and to investigate the asymptotic behaviour of the flow. Although a higher-order perturbation analysis is the natural extension of linear theory, it is not only limited for our purposes, but also very difficult to implement. Thus, we base our analysis on an efficient method for solving Euler's equation, exploiting the particularly simple (linear) form of the vorticity distribution. We formulate the problem as a nonlinear integrodifferential equation for the vortex contour separating rotational from irrotational fluid. This equation is solved numerically, using a high-order discretization of the vortex contour. A similar method has been successfully employed for studying vorticity dynamics in two dimensions (Deem & Zabusky 1978; Pozrikidis & Higdon 1985).

In §2 we present the mathematical formulation and in §3 we develop the numerical procedure. Results for the nonlinear evolution of Hill's vortex with axisymmetric spheroidal perturbations are presented and discussed in §§4 and 5.

2. Mathematical formulation

We consider inviscid, axisymmetric flow without swirl, and refer to cylindrical polar coordinates (x, σ, φ). For the kinematics of the flow field it is convenient to introduce the Stokes stream function, defined by the equation

$$\boldsymbol{u} = (u, v, 0) = \nabla \times \left(\frac{\psi}{\sigma}\hat{\boldsymbol{k}}\right) = \frac{1}{\sigma}\left(\frac{\partial \psi}{\partial \sigma}, -\frac{\partial \psi}{\partial x}, 0\right). \tag{1}$$

The vorticity $\boldsymbol{\omega} = \nabla \times \boldsymbol{u}$ is directed in the azimuthal direction, $\boldsymbol{\omega} = (0, 0, \omega)$; the vortex lines are concentric circles, centred on the axis of symmetry. In terms of the stream function, the vorticity may be written

$$\omega = -\frac{1}{\sigma}\left(\frac{\partial^2 \psi}{\partial x^2} + \frac{\partial^2 \psi}{\partial \sigma^2} - \frac{1}{\sigma}\frac{\partial \psi}{\partial \sigma}\right). \tag{2}$$

This is a Poisson equation which can be readily inverted to yield the stream function in terms of the vorticity distribution (Lamb 1932 art. 161),

$$\psi(\boldsymbol{x}_0) = \frac{\sigma_0}{4\pi}\int \frac{\sigma}{r}\cos(\varphi_0 - \varphi)\,\omega\,\mathrm{d}\sigma\,\mathrm{d}x\,\mathrm{d}\varphi + \psi_{\mathrm{E}}(\boldsymbol{x}_0), \tag{3}$$

where $r = |\boldsymbol{x}_0 - \boldsymbol{x}|$, and ψ_{E} expresses an external irrotational flow. This equation

views the flow as the result of the fundamental motions induced by the vorticity. The integration may be performed with respect to φ to yield

$$\psi(\boldsymbol{x}_0) = \int G\omega \,\mathrm{d}\sigma \,\mathrm{d}x + \psi_{\mathrm{E}}(\boldsymbol{x}_0), \tag{4}$$

where

$$G = \frac{1}{2\pi}(\sigma\sigma_0)^{\frac{1}{2}}\left[\left(\frac{2}{k}-k\right)K(k) - \frac{2}{k}E(k)\right], \tag{5}$$

with

$$k^2 = \frac{4\sigma\sigma_0}{(x-x_0)^2+(\sigma+\sigma_0)^2}.$$

$G(x-x_0, \sigma, \sigma_0)$ is the stream function associated with a circular vortex ring of unit strength, and K and E are the complete elliptic integrals of the first and second kind. The integration in (4) is over any semi-infinite axial plane, bounded by the x-axis. Using (1) we may write

$$\boldsymbol{u}(\boldsymbol{x}_0) = \int \nabla_0 \times \left(\frac{G\omega}{\sigma}\hat{\boldsymbol{k}}\right)\mathrm{d}\sigma \,\mathrm{d}x + \boldsymbol{u}_{\mathrm{E}}(\boldsymbol{x}_0), \tag{6}$$

where $\boldsymbol{u}_{\mathrm{E}} = \nabla_0 \times (\psi_{\mathrm{E}}\hat{\boldsymbol{k}}/\sigma)$, and ∇_0 denotes differentiation with respect to x_0, σ_0.

We assume now that the vorticity is concentrated within a closed axisymmetric region, and vanishes outside this region. Further, we assume that within the rotational region, the vorticity is independent of the axial position x, $\omega = \omega(\sigma)$. Under these conditions, we may use Stokes theorem to express the v component in (6) as

$$\begin{aligned} v(\boldsymbol{x}_0) &= -\frac{1}{\sigma_0}\frac{\partial}{\partial x_0}\int G\omega \,\mathrm{d}\sigma \,\mathrm{d}x + v_{\mathrm{E}}(\boldsymbol{x}_0) \\ &= \frac{1}{\sigma_0}\int \frac{\partial}{\partial x}(G\omega)\,\mathrm{d}\sigma \,\mathrm{d}x + v_{\mathrm{E}}(\boldsymbol{x}_0) = \frac{1}{\sigma_0}\oint_{C_{\mathrm{v}}} G\omega \hat{\boldsymbol{j}}\cdot\hat{\boldsymbol{t}}\,\mathrm{d}l + v_{\mathrm{E}}(\boldsymbol{x}_0), \end{aligned} \tag{7}$$

where C_{v} is the projection of the vortex contour on an axial plane, $\hat{\boldsymbol{t}}$ is the unit tangent to C_{v}, and the integral is taken in the counterclockwise sense.

One might attempt to write an analogous expression for the u component of the velocity, but this is prohibited by the non-symmetric functional dependence of the fundamental solution G on σ and σ_0. To surmount this difficulty, we note that the flow outside the vortex is irrotational, and introduce the potential function $\phi(x-x_0, \sigma, \sigma_0)$, defined by the equation

$$\boldsymbol{u} = \nabla\phi. \tag{8}$$

By analogy with (4), we express ϕ as an integral over the vorticity distribution,

$$\phi(\boldsymbol{x}_0) = \int F\omega \,\mathrm{d}\sigma \,\mathrm{d}x + \phi_{\mathrm{E}}(\boldsymbol{x}_0). \tag{9}$$

$F = -\Omega/4\pi$ is the velocity potential associated with a circular vortex ring of unit strength, proportional to the solid angle Ω subtended by the ring from the point (x_0, σ_0) (Batchelor 1967 §2.6), and ϕ_{E} expresses an external irrotational flow. Differentiating (9) with respect to x_0 and applying Stokes theorem as in (7), we write u as a contour integral over C_{v}

$$\begin{aligned} u(\boldsymbol{x}_0) &= \frac{\partial}{\partial x_0}\int F\omega \,\mathrm{d}\sigma \,\mathrm{d}x + u_{\mathrm{E}}(\boldsymbol{x}_0) \\ &= -\int \frac{\partial}{\partial x}(F\omega)\,\mathrm{d}\sigma \,\mathrm{d}x + u_{\mathrm{E}}(\boldsymbol{x}_0) = -\oint_{C_{\mathrm{v}}} F\omega \hat{\boldsymbol{j}}\cdot\hat{\boldsymbol{t}}\,\mathrm{d}l + u_{\mathrm{E}}(\boldsymbol{x}_0). \end{aligned} \tag{10}$$

It is important to note that F is multiple valued and thus, application of (9) or (10) requires a branch cut at $x = x_0$, $\sigma > \sigma_0$. Once this branch cut is introduced the above equations are uniformly valid throughout the flow.

Summarizing, we write the velocity in the integral form

$$\boldsymbol{u}(\boldsymbol{x}_0) = \oint_{C_v} \boldsymbol{P}\omega(\sigma)\hat{\boldsymbol{j}}\cdot\hat{\boldsymbol{t}}\,\mathrm{d}l + \boldsymbol{u}_{\mathrm{E}}(\boldsymbol{x}_0), \tag{11}$$

where $\boldsymbol{P} = (G, -F, 0)$ is specified by (5) and (9), and the flow field $\boldsymbol{u}_{\mathrm{E}}$ is irrotational. According to this equation, the velocity at any point in the flow is specified by the position and the vorticity of the fluid particles along the vortex contour.

Equation (11) expresses a kinematic condition, valid at an initial instant where ω is independent of x. To extend this equation at later times, we require that ω remains independent of x during the motion. Thus, we consider the dynamic condition expressed by the vorticity transport equation. This equation for homogeneous or barotropic and incompressible fluids in axisymmetric flow takes the form

$$\frac{\mathrm{D}}{\mathrm{D}t}\left(\frac{\omega}{\sigma}\right) = 0, \tag{12}$$

where $\mathrm{D}/\mathrm{D}t$ indicates a material derivative. We observe that $\omega = \lambda\sigma$, where λ is a constant, is a steady solution to this equation, implying that if the vorticity is a linear function of σ at an initial instant, it will remain so throughout the evolution. The physical mechanism underlying this solution is the following; when a material vortex ring is stretched so that its radius increases by a certain factor, its vorticity increases by the same factor owing to vortex stretching. Examples of flows with linear vorticity distribution include the members of the family of steady vortices described by Norbury (1973).

Substituting $\omega = \lambda\sigma$ into (11) and evaluating for fluid particles on the vortex contour yields a highly nonlinear integrodifferential equation for the trajectories of these particles $\boldsymbol{x}(\alpha, t)$

$$\frac{\partial \boldsymbol{x}}{\partial t} = \lambda \int_0^A \boldsymbol{P}\sigma\hat{\boldsymbol{j}}\cdot\hat{\boldsymbol{t}}\frac{\partial l}{\partial \alpha}\,\mathrm{d}\alpha + u_{\mathrm{E}}(\boldsymbol{x}), \tag{13}$$

where α is a Langrangian variable, $0 \leqslant \alpha \leqslant A$. This equation may be used for the efficient calculation of steady axisymmetric vortices, in a procedure similar to that used by Pierrehumbert & Widnall (1981), or Saffman & Szeto (1981) in two dimensions. More importantly for our purposes, this equation may also be used to study the evolution of unsteady vortices.

3. Numerical procedure

We implement our numerical procedure by identifying a collection of marker points on the vortex contour. The initial velocity at each point is calculated by interpolating for the position of the vortex contour as discussed below. The computation proceeds forward in time via a fourth-order Runge–Kutta procedure.

A direct numerical evaluation of the contour integral for the v velocity component is prohibited by the singular behaviour of the kernel G. As $x \to x_0$ and $\sigma \to \sigma_0$, $k \to 1$ and $G \to S = \sigma_0 \ln(4/(1-k^2)^{\frac{1}{2}})/2\pi$. To remove the singularity we write

$$v(\boldsymbol{x}_0) = \frac{\lambda}{\sigma_0}\int (G\sigma - S\sigma_0)\hat{\boldsymbol{j}}\cdot\hat{\boldsymbol{t}}\,\mathrm{d}l + \lambda\int S\hat{\boldsymbol{j}}\cdot\hat{\boldsymbol{t}}\,\mathrm{d}l. \tag{14}$$

The first integral is evaluated numerically using a Gauss–Legendre quadrature, as explained below. The second integral may be evaluated exactly over elementary segments such as straight lines or circular arcs. The choice of circular arcs passing through three successive points, yields higher accuracy without requiring a complicated implementation.

For the evaluation of the u velocity component, we calculate the solid angle Ω in terms of complete elliptic integrals of the third kind $\pi(\varphi/k^2)$; these may be expressed in terms of complete and incomplete elliptic integrals of the first and second kind (Abramowitz & Stegun 1972 p. 589), which in turn may be efficiently computed using an iterative procedure (Davis 1960). Thus,

$$\left.\begin{aligned} \Omega = 2\pi\frac{x-x_0}{|x-x_0|} - \frac{1}{B}\frac{x_0-x}{((x_0-x)^2+(\sigma_0+\sigma)^2)^{\frac{1}{2}}}[(C+1)\,n_1\,\pi(-n_1/k^2) \\ -(C-1)\,n_2\,\pi(n_2/k^2)], \\ \text{where,} \quad B = \frac{\sigma_0}{((x_0-x)^2+\sigma_0^2)^{\frac{1}{2}}}, \quad C = \frac{\sigma}{((x_0-x)^2+\sigma_0^2)^{\frac{1}{2}}}, \\ n_1 = \frac{2B}{(1-B)}, \quad n_2 = \frac{2B}{(1+B)}. \end{aligned}\right\} \tag{15}$$

The regular contour integrations of the first integral in (14) as well as the contour integral for the u velocity are performed over sets of circular arcs connecting adjacent trios of points, using a Gauss–Legendre quadrature. The number of nodes in the quadrature is evaluated separately for each arc by specifying a maximum integration step.

After each timestep, the distribution of points is examined, and points are inserted or removed according to the criteria established by Pozrikidis & Higdon (1985). Briefly, the procedure includes insertion of points at regions of high curvature or low point concentration, and removal of points in low-curvature regions.

To monitor the accuracy of our calculations, after each timestep we calculate the vortex volume and fluid impulse, both invariants of the motion (the mathematical definition of these quantities is given later in our discussion). In all of the calculations, the maximum change in each invariant, due to numerical error, was of the order of 0.1 %. Further, as an independent test of accuracy, we repeated selected calculations using half the number of points and relaxing the point insertion criteria by a factor of two. The results were visually indistinguishable, indicating that the error was indeed kept small.

The computations presented in this work were performed on a VAX-11/780 computer equipped with an FPS-164 processor. Typical CPU time for a complete run was of the order of 3 h.

4. The evolution of Hill's vortex

4.1. *The unperturbed state*

In a frame of reference which moves with the vortex, the flow inside Hill's vortex is specified by the stream function

$$\psi = \frac{\lambda}{10}\sigma^2(a^2-r^2), \tag{16}$$

where $r^2 = x^2+\sigma^2$, and a is the vortex radius (Lamb 1932 art. 165). The corresponding

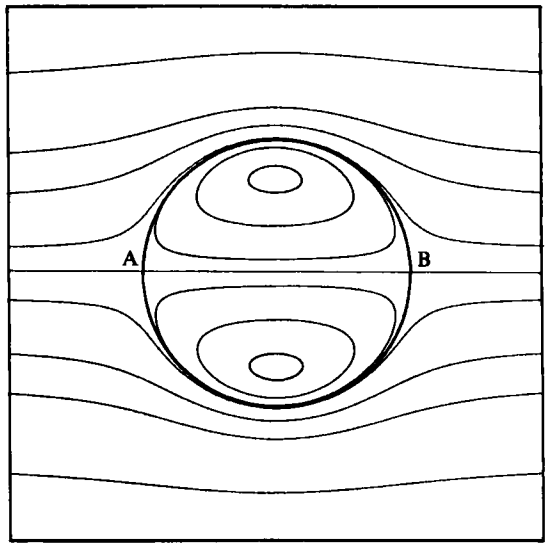

FIGURE 1. Streamline pattern of Hill's spherical vortex. The vorticity inside the vortex increases linearly in the radial direction, $\omega = \lambda\sigma$; the speed of the approaching stream is $U = -\frac{2}{15}\lambda a^2$. In our discussion we assume $\lambda < 0$ and thus, we refer to A as the front, and to B as the rear stagnation point.

streamline pattern is presented in figure 1. The above stream function yields a sinusoidal variation of the tangential velocity on the vortex surface, suggesting that the irrotational flow outside the vortex may be taken as a uniform flow past a sphere,

$$\psi = \tfrac{1}{2}U\sigma^2\left(1-\frac{a^3}{r^3}\right). \tag{17}$$

Continuity of velocity (and hence of pressure) across the vortex surface requires that

$$U = -\tfrac{2}{15}\lambda a^2. \tag{18}$$

Equations (16) to (18) provide a complete specification of the undisturbed flow. In an alternative fashion, one may use (11) to express the velocity as a contour integral, where $\omega = \lambda\sigma$, $\boldsymbol{u}_{\mathrm{E}} = \hat{\imath}U$, and the contour C_{v} is a semi-circle along the vortex boundary.

4.2. *Linear analysis*

Bliss (1973) formulated the linear problem for small axisymmetric perturbations. His analysis was extended by Moffatt & Moore (1978) who gave an approximate solution to the system of infinite coupled ordinary differential equations for the motion of the vortex boundary. In a frame of reference moving with the unperturbed vortex speed U, the vortex boundary is specified in spherical coordinates as

$$r = a(1+\epsilon h(\theta, t)), \tag{19}$$

where h is expansible in a series involving Legendre polynomials

$$h = \sum_{0}^{\infty} h_n(t)\, P_n(\mu) = -\frac{2}{15}\sum_{1}^{\infty} (2n+1)\, A_n(t)\, P_n'(\mu), \tag{20}$$

with $\mu = \cos\theta$. The coefficients $A_n(t)$ are calculated in closed form with a maximum

error 2%. Emphasis is placed on the initial conditions $h_n(0) = 0$ for $n \neq 2$, and $h_2(0) = 1$, corresponding to spheroidal perturbations. Considering the behaviour as $Ut/a \gg 1$, while $Ut/a \ll \frac{1}{3}\ln(10/\epsilon)$, the authors showed that for prolate disturbances, the vortex detrains a fraction $\frac{2}{5}\epsilon$ of its volume, in the form of a thin spike growing from the rear stagnation point. The disturbance velocity is not strong enough to deform the spherical shape of the remaining vortex of reduced radius $a(1-\frac{1}{5}\epsilon)$. At large times, the vortex translates downstream as a slow speed $\frac{2}{5}\epsilon U$. For oblate disturbances, irrotational fluid is entrained into the vortex from the rear stagnation point. This results in an increase of the vortex radius by a factor of $\frac{1}{5}\epsilon$. Moffatt & Moore suggested that the entrained fluid reaches the front stagnation point, and then circulates within the vortex in a spiral pattern. In this fashion, the vortex reduces to a vortex ring which slowly translates upstream at a speed $\frac{2}{5}\epsilon U$.

4.3. *Nonlinear evolution*

We consider disturbances similar to those used by Moffatt & Moore, equations (19), (20), where at the initial instant $h_2(0) = 1$ is the only non-zero perturbation coefficient. In addition, we require that the original vortex volume $V = \frac{4}{3}\pi a^3$ is preserved, where a is the undisturbed vortex radius. The vorticity transport equation (13) indicates that for linear vorticity distribution, conservation of volume implies conservation of circulation. Thus, preserving the vortex volume guarantees that the disturbance flow is irrotational. Our initial conditions are

$$r = a\gamma(a + \epsilon h_2), \tag{21}$$

where γ is a function of ϵ, so that the vortex volume is preserved. ϵ expresses the deviation from the spherical shape; positive ϵ correspond to prolate, while negative ϵ to oblate perturbations.

We discuss the evolution in terms of the non-dimensional time $t^* = Ut/a$, where U may be viewed either as the speed of the undisturbed vortex translating in a quiescent fluid, or as the speed of a uniform fluid past a steady vortex.

To start, we consider the evolution of a small amplitude prolate perturbation, $\epsilon = 0.050$, illustrated in figure 2. In the initial stage, a certain amount of rotational fluid is convected to the rear of the vortex, as shown in figure 2(*b*). The front of the vortex obtains a nearly spherical shape, in agreement with predictions of linear analysis. The fluid accumulated at the rear of the vortex is elongated under the influence of the local stagnation point flow and forms a vortex tail, figure 2(*c*). Meanwhile, due to detrainment of rotational fluid, the main vortex starts translating downstream (to the right in a frame of reference that moves with the unperturbed vortex speed). As time proceeds, the vortex tail suffers continuous elongation, primarily under the influence of the flow induced by the spherical core. The region connecting the tail to the main vortex is pinched by the local stagnation point flow and its thickness decreases at an exponential rate, figure 2(*d*). Figure 2(*e*) is illustrative of the asymptotic behaviour, in which the tail tends to separate from the main spherical vortex and to form an independent entity with low circulation.

To resolve the nature of the asymptotic motion, we examine the change in the size of the vortex core during the evolution. For this purpose, we define the radius of the core r_c, as the maximum displacement in the radial direction, $r_c = \sigma(x_c) = \max(\sigma)$, where x_c is defined as the centre of the core. In figure 3 we plot the non-dimensional $r_c^* = 5(1-r_c/a)/\epsilon$, as a function of time t^*. At large times, r_c tends to an asymptotic value indicating that the core is not being depleted of rotational fluid. This asymptotic value is accurately predicted by linear analysis to be equal to

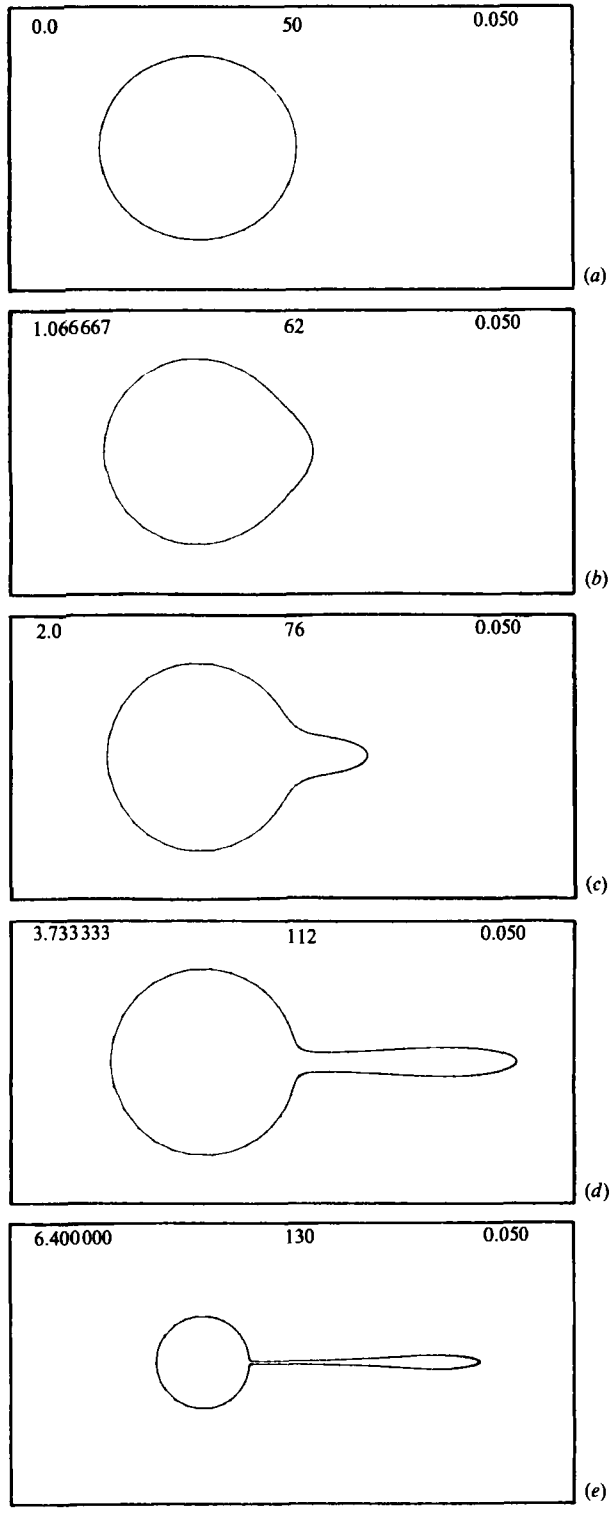

FIGURE 2. Evolution of vortex with small-amplitude prolate perturbation, $\epsilon = 0.050$. Numbers at top of each frame give time $t^* = Ut/a$, number of marker points along the contour, and ϵ. The scale in frame (*e*) is reduced by a factor of 2; (*a*) $t^* = 0$, (*b*) 1.067, (*c*) 2.000, (*d*) 3.733, (*e*) 6.400.

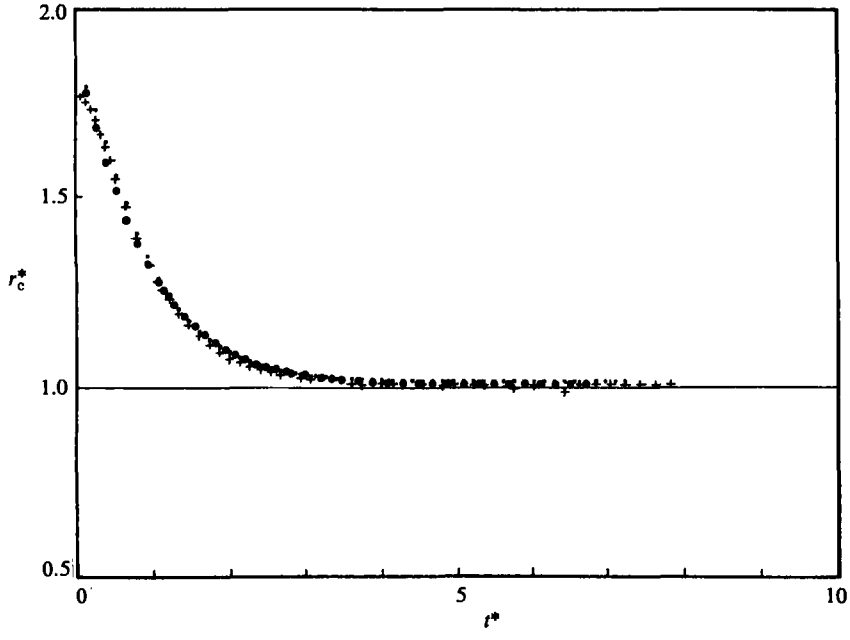

FIGURE 3. The normalized core radius $r_c^* = 5(1-r_c/a)/\epsilon$, as a function of time t^*, for prolate perturbations. Linear analysis predicts that at large times $r_c^* \to 1$: (*a*) +, $\epsilon = 0.050$; (*b*) ., 0.150; (*c*) ●, 0.300.

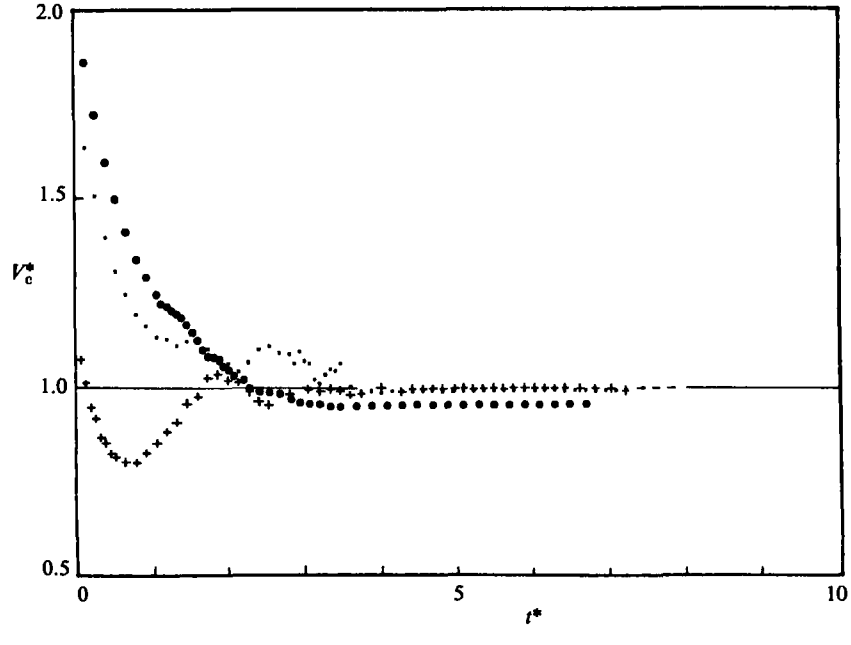

FIGURE 4. The normalized core volume $V_c^* = 5(1-V_c/V)/3\epsilon$, as a function of time t^*, for prolate perturbations; V is the total vortex volume. Linear analysis predicts that at large times $V_c^* \to 1$: (*a*) +, $\epsilon = 0.050$; (*b*) ., 0.150; (*c*) ●, 0.300.

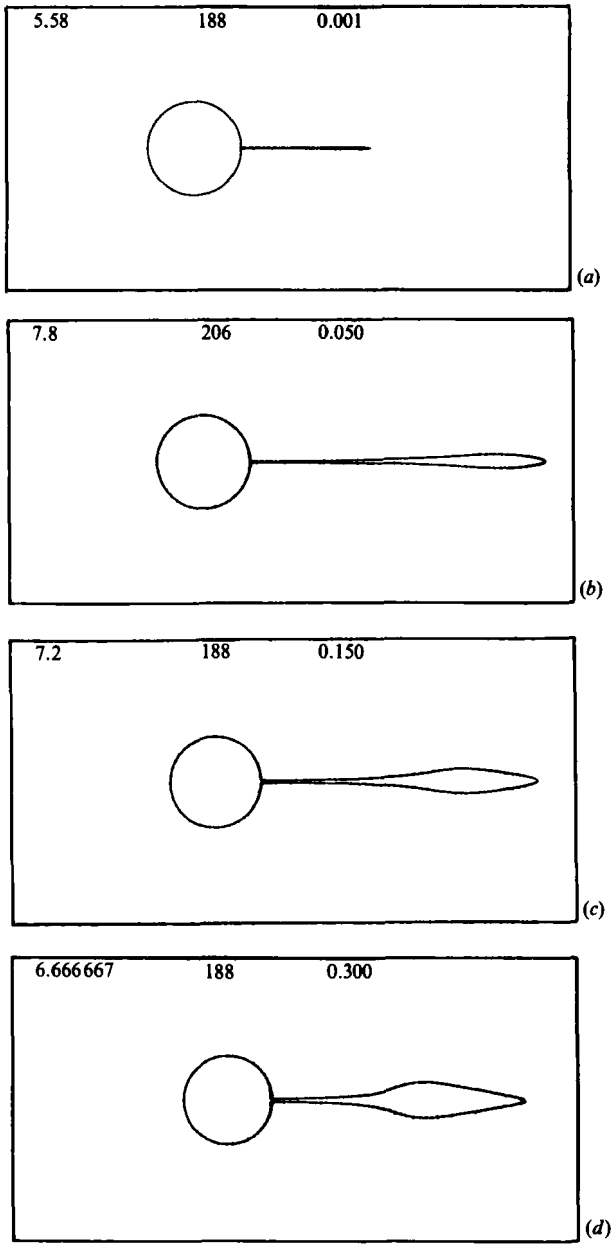

FIGURE 5. Advanced stages of vortex for prolate perturbations of different initial amplitude: (*a*) $\epsilon = 0.001$, $t^* = 5.580$; (*b*) $\epsilon = 0.050$, $t^* = 7.800$; (*c*) $\epsilon = 0.150$, $t^* = 7.200$; (*d*) $\epsilon = 0.300$, $t^* = 6.667$.

$(1-\frac{1}{5}\epsilon)\,a = 0.990a$. Another measure of the detrainment is the volume of the vortex core between the planes $x = x_F$ and $x = x_F + 2r_c$, where x_F is the front of the vortex. Figure 4 shows that V_c tends to an asymptotic value verifying that fluid is not detrained from the core. This asymptotic value is again closely predicted by linear analysis to be equal to $V_c = (1-\frac{3}{5}\epsilon)V = 0.970\ V$, where V is the total vortex volume. To examine the shape of the core, we compare the separation between the core centre

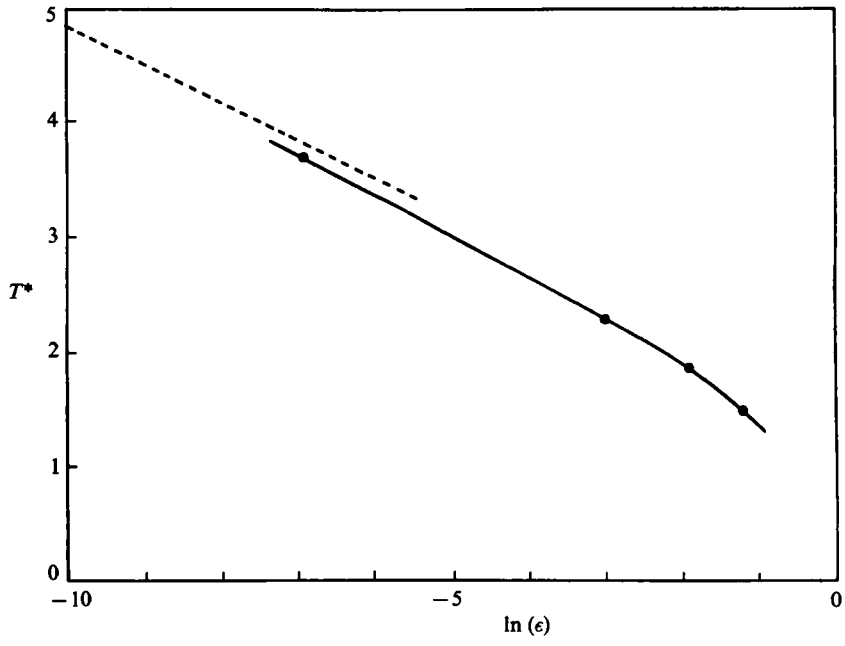

FIGURE 6. Dimensionless time $T^* = UT/a$ at which the vortex tail travels a distance equal to one vortex radius downstream, as a function of the log of the initial amplitude of the disturbance, ln (ϵ); the dashed line shows predictions of linear theory.

and the front stagnation point, $x_c - x_F$, to the core radius r_c. In the advanced evolution stages these are identical, suggesting a spherical core.

The evolution of prolate perturbations of larger initial amplitude is similar to that described above, although the motion is governed by nonlinear effects from the initial stages. This involves accumulation of fluid at the rear stagnation point, and formation of a spherical core and adjoining vortex tail. Disturbances of initial amplitude larger than 0.300 are of minor physical interest, as they require an irregular initial deformation of the vortex boundary. On the other hand, the evolution with very small disturbances is adequately described by linear analysis (even at large times), and is similar to that presented above. Figure 5 shows typical advanced stages in the evolution for amplitudes $\epsilon = 0.001, 0.050, 0.150$ and 0.300. The corresponding behaviour of the core radius r_c and core volume V_c are shown in figures 3 and 4. These figures suggest that the initial amplitude ϵ is an important parameter for the evolution, as it determines not only the growth rate of the perturbation but also the size of the developing vortex tail. As ϵ is increased, a larger fraction of rotational fluid detrains from the vortex to form the vortex tail. This is in agreement with linear predictions. To assess the effect of ϵ on the growth rate of the disturbance, we consider the time T at which the vortex tail reaches a position equal to one vortex radius downstream. In figure 6 we plot $T^* = UT/a$ as a function of ln (ϵ). The dashed line, $T^* = 1.517 - \frac{1}{3}\ln(\epsilon)$, is derived from linear analysis by Moffatt & Moore, and shows the behaviour for infinitesimal perturbations.† As expected, larger initial deformations induce a stronger disturbance flow with a faster downstream convection of the vortex tail.

† The equation $T^* = 2.592 - \frac{1}{3}\ln(\epsilon)$ given by Moffatt & Moore is erroneous, owing to error in numerical integration.

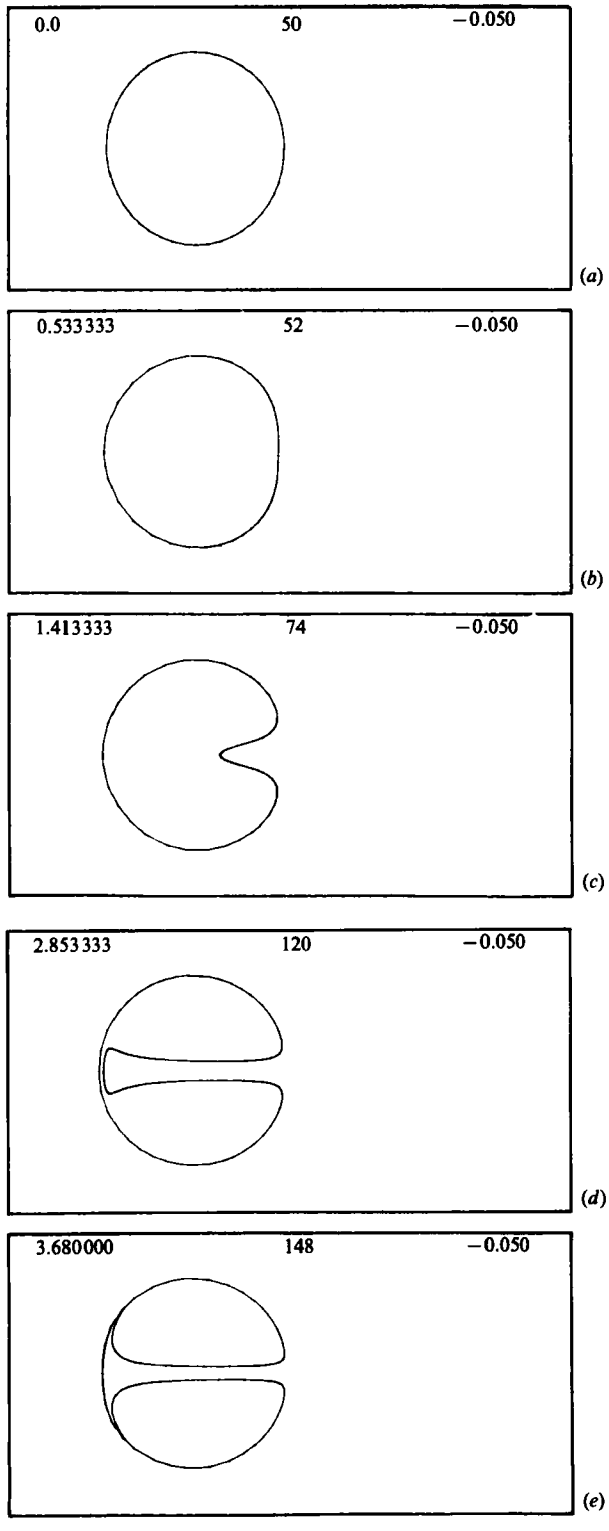

FIGURE 7. For caption see p. 350.

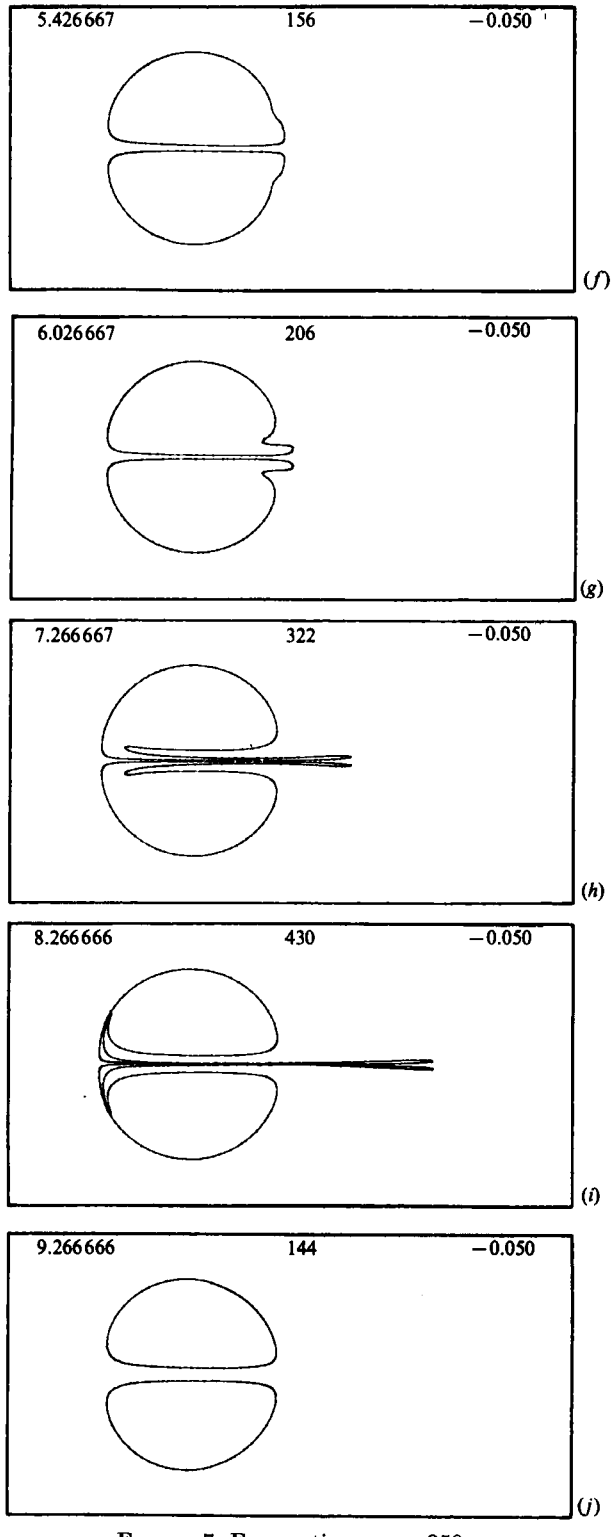

FIGURE 7. For caption see p. 350.

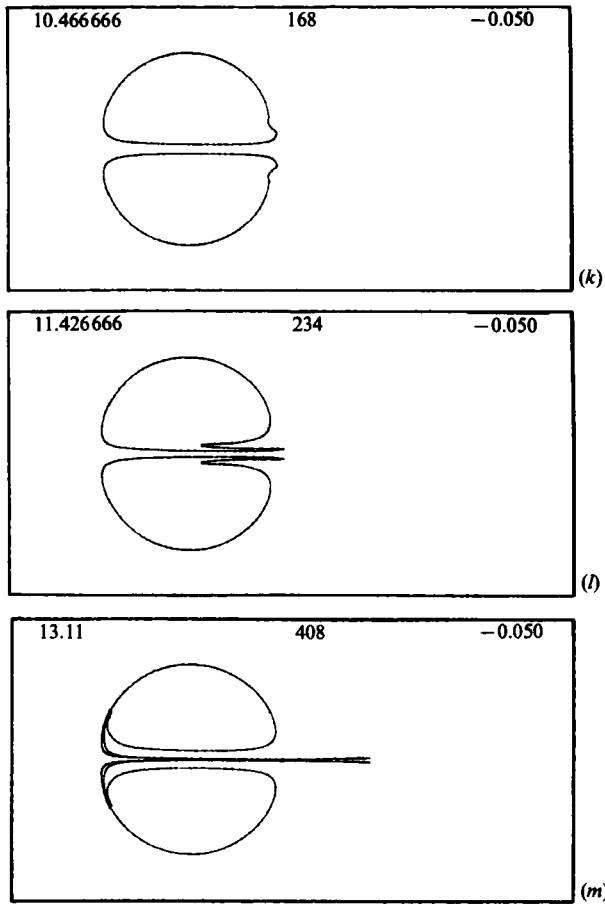

FIGURE 7. Evolution of vortex with small-amplitude oblate perturbation, $\epsilon = -0.050$: (*a*) $t^* = 0$; (*b*) 0.533; (*c*) 1.413; (*d*) 2.853; (*e*) 3.680; (*f*) 5.427; (*g*) 6.027; (*h*) 7.267; (*i*) 8.267; (*j*) 9.267; (*k*) 10.467; (*l*) 11.427; (*m*) 13.110.

Continuing our discussion, we consider oblate perturbations, beginning with a small amplitude disturbance $\epsilon = -0.050$ (figure 7). Initially, the disturbed rotational fluid near the vortex surface moves towards the front of the vortex, restoring its spherical shape in agreement with linear predictions. By conservation of rotational fluid, this results in a flattening of the vortex near the rear stagnation point (figure 7*b*). This is followed by convection of irrotational fluid into the vortex causing an expansion of the vortex (figure 7*c*). The entrained fluid moves along the axis of symmetry, and approaches close to the front vortex boundary (figure 7*d*). In this fashion, the spherical vortex reduces to a vortex ring. The closed streamlines in the interior of the vortex cause the entrained irrotational fluid to circulate along the vortex contour, bounded by an infinitesimal thin spherical filament of rotational fluid, figure 7 (*e*). This completes the first stage of the evolution. In later stages, the vorticity in the spherical filament is eliminated for computational efficiency. As will be discussed later, this simplification did not affect the accuracy of our results. Thus, while deleting this vorticity decreased the flow circulation impulse and energy by approximately 0.15%, it substantially reduced the number of marker points by 28%. Similar contour simplifications will be employed in the rest of the calculations presented in this

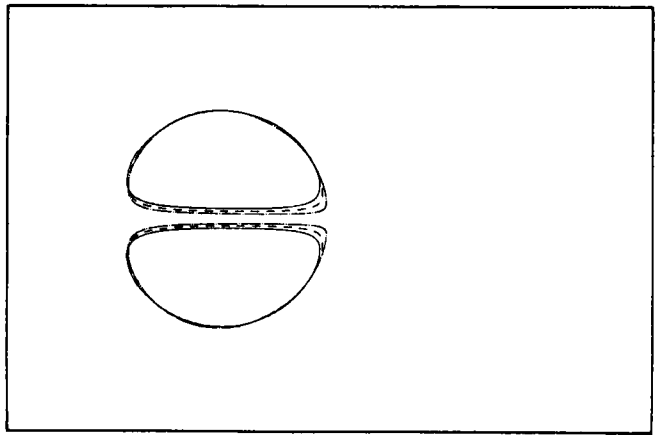

FIGURE 8. The shape of the vortex ring developed from a small amplitude oblate perturbation, $\epsilon = -0.050$: –·–, $t^* = 4.507$; – – –, $t^* = 9.266$; ——, $t^* = 13.110$.

section. Continuing with the evolution, we note that the vortex ring shown in figure 7 (*e*) is nearly symmetric with respect to the vertical plane passing through its centre. Further, by comparing figures 7 (*e*), (*f*) we conclude that the vortex ring evolves at a slow rate. Thus, we may identify the further evolution of the vortex with the evolution of a perturbed, steady and symmetric vortex ring (the structure and properties of such rings are discussed in the next section). Figure 7 (*f*) shows that the 'excess' rotational fluid responsible for the asymmetry of the ring takes the form of a wave on the surface of the vortex, which is convected by the outer flow to the rear stagnation point. A portion of this 'excess' fluid is convected downstream by the outer flow in the form of a thin vortex tail (figure 7*g*). At the same time, a thin layer of irrotational fluid is entrained into the vortex just above the vortex tail. At later times, the tail is stretched by the external flow and loses its dynamic significance (figure 7*h*, *i*). On the other hand, the entrained fluid reaches the front of the vortex and circulates along the ring boundary forming a thin, axisymmetric vortex filament. If the initial spherical vortex filament had not been deleted (figure 7*e*), it would form a continuation of this filament in a spiral pattern. In the end of this evolution period (figure 7*i*), the vortex is reduced into a system of two compact structures; the primary, nearly symmetric vortex ring and a small secondary toroidal vortex at the front of the vortex ring. The two structures are connected with the above thin vortex filament. Recalling that the circulation of each structure is proportional to its volume, it is easy to see that the circulation of the secondary vortex is much smaller than that of the ring. For the pattern shown in figure 7 (*i*), the circulation, impulse and energy of the secondary vortex account for approximately 1 % of the total flow properties. This indicates that the secondary vortex is of minor dynamic significance and thus, it can be deleted for computational efficiency. It is important to note that if the secondary vortex is not deleted, it will be stretched by the elongational flow at the front stagnation point and its vorticity will be convected into the main vortex ring. Thus, its significance will be reduced even more during the evolution. Continuing with the evolution we note the similarity between the profiles shown in figures 7 (*i*), (*e*). As a result of this similarity, the vortex repeats the above evolution cycle, forming a new vortex tail and entraining a new thin filament of irrotational fluid around the primary vortex ring (compare figures 7*j–m* to 7*e–i*). In the end of this cycle, the vortex

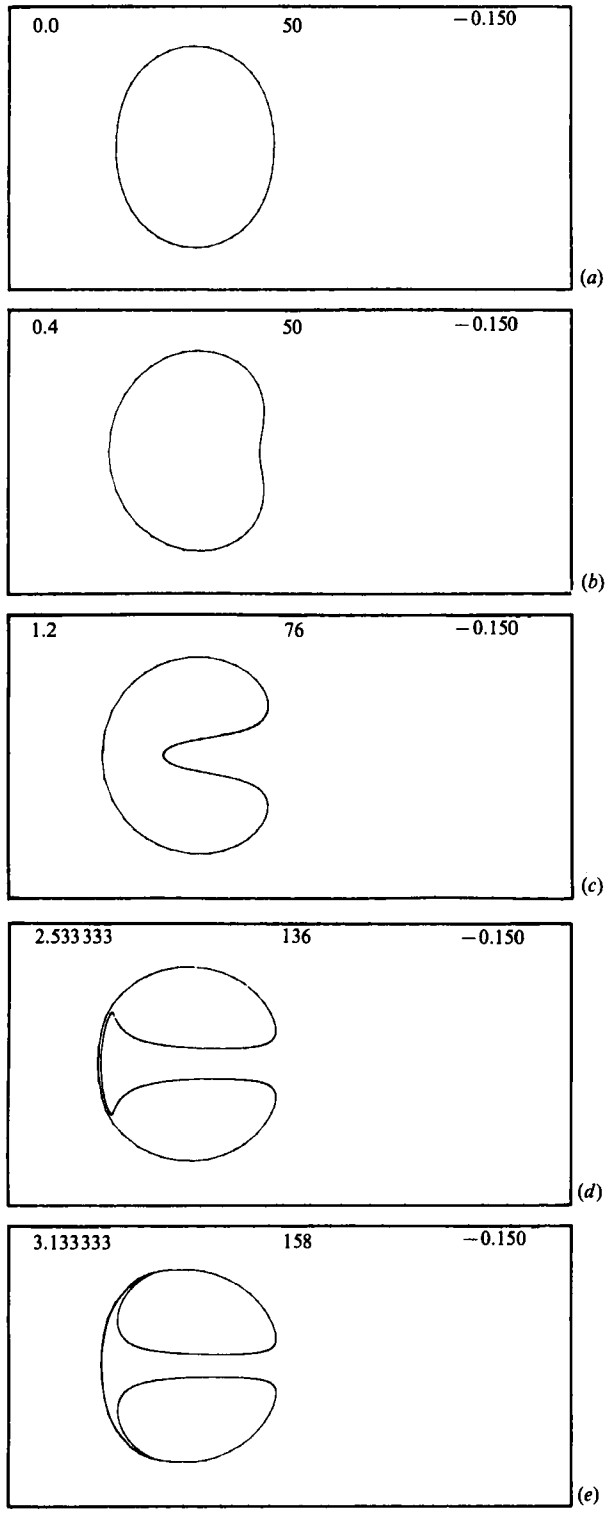

FIGURE 9. For caption see p. 354.

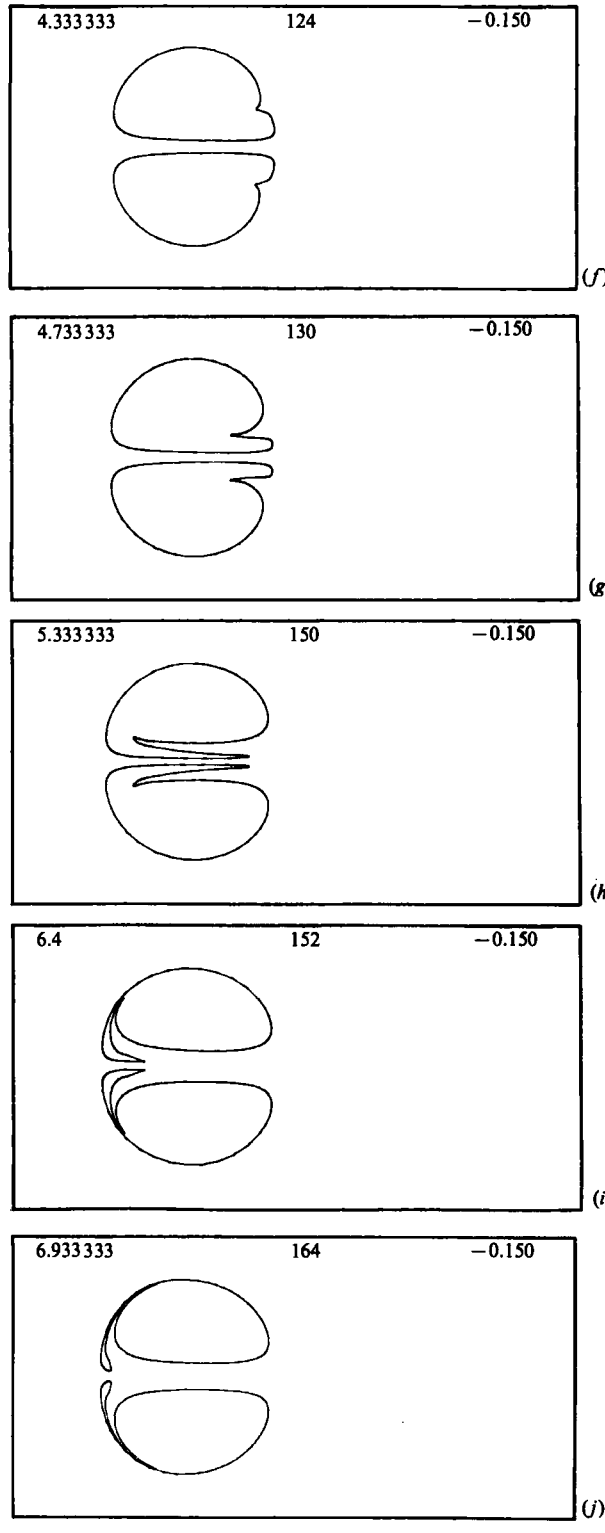

FIGURE 9. For caption see p. 354.

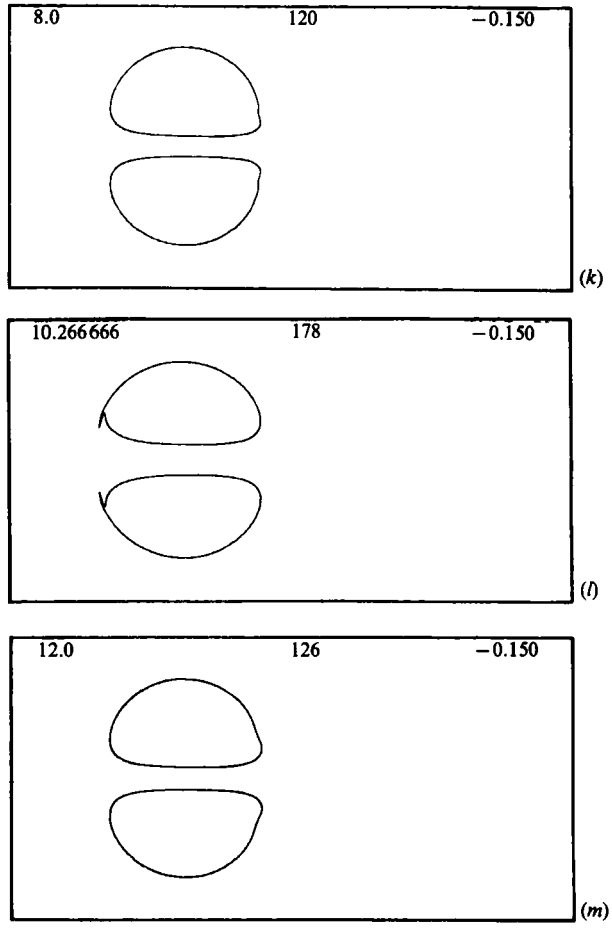

FIGURE 9. Evolution of vortex with an oblate perturbation of initial amplitude $\epsilon = -0.150$: (*a*) $t^* = 0$; (*b*) 0.400; (*c*) 1.200; (*d*) 2.533; (*e*) 3.133; (*f*) 4.333; (*g*) 4.733; (*h*) 5.533; (*i*) 6.400; (*j*) 6.933; (*k*) 8.000; (*l*) 10.267; (*m*) 12.000.

ring obtains a shape similar to that described previously in figures 7(*e*), (*k*). To facilitate the comparison, we superimpose the ring boundary at three different times in figure 8. The notable similarity between the patterns in this figure suggests that once again, the above evolution cycle will be repeated. In this fashion, the flow will tend to an asymptotic state in which the entrained irrotational fluid will form successive thin vortex filaments around a nearly steady vortex ring.

The evolution for small amplitude oblate perturbation discussed above is consistent with linear analysis. To investigate the effect of finite amplitude, we consider the motion for $\epsilon = -0.150$, illustrated in figure 9. This is similar to that for $\epsilon = -0.050$, involving the development of a nearly steady vortex ring (figure 9*a–e*), whose slow evolution leads to the formation of a thin vortex filament in a spiral pattern (figure 9*f–i*). The contour surgery performed at the stage shown in figure 9*e* resulted in approximately 1 % reduction in the flow properties. The ring diameter is now larger (compare figures 7*e*, 9*e*) and thus, the cross-section of the vortex is smaller, owing to conservation of volume. As a difference from the $\epsilon = -0.050$ evolution, we observe that the 'excess' fluid at the rear stagnation point does not form a vortex tail (figure

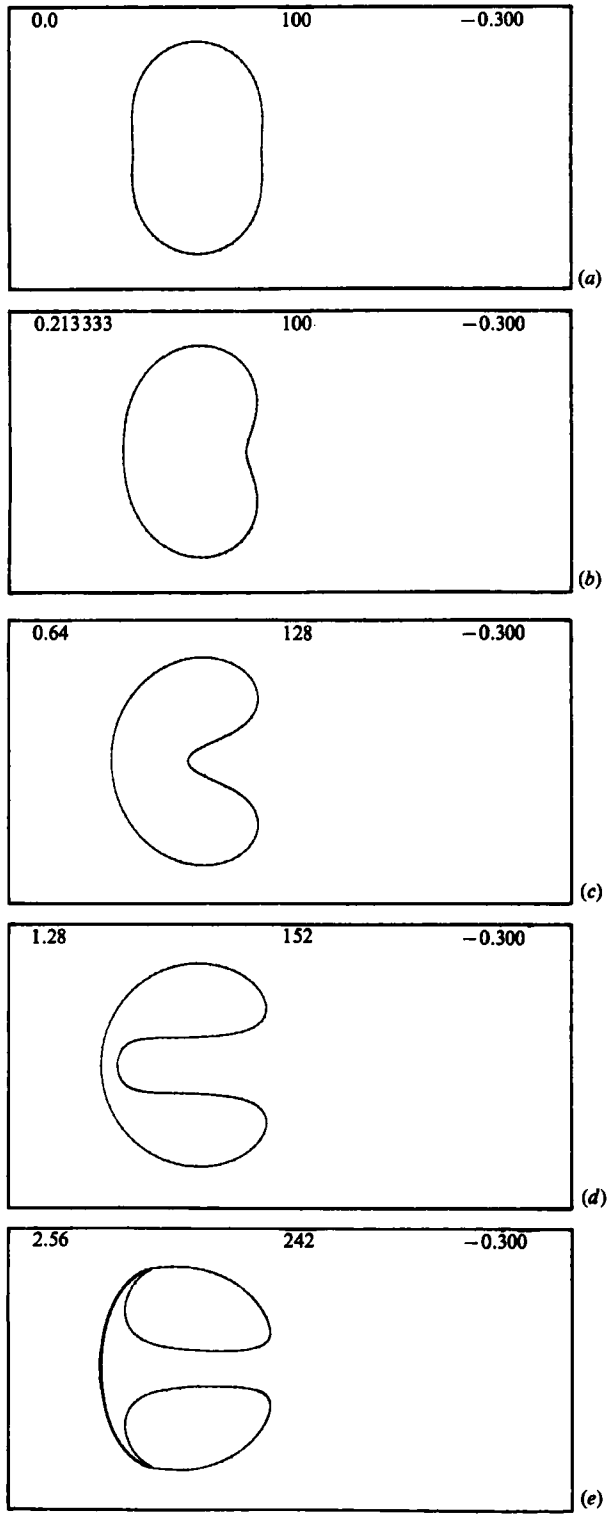

FIGURE 10. For caption see p. 357.

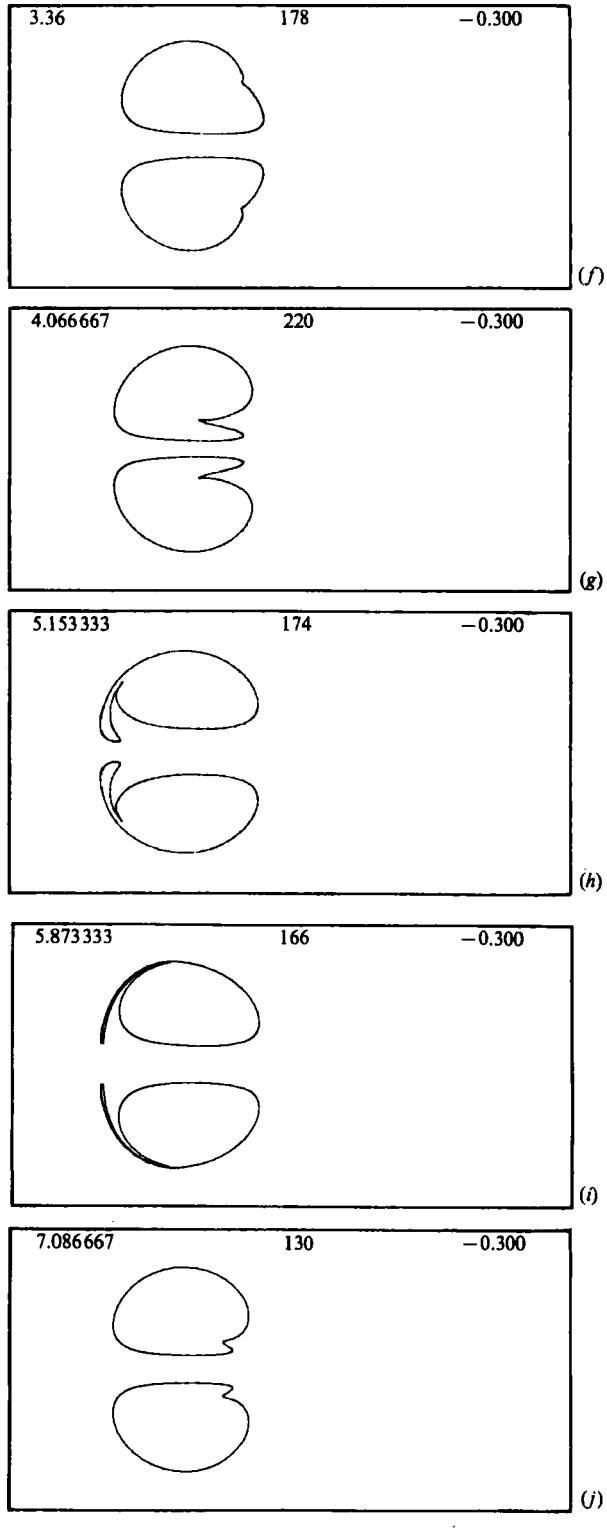

FIGURE 10. For caption see facing page.

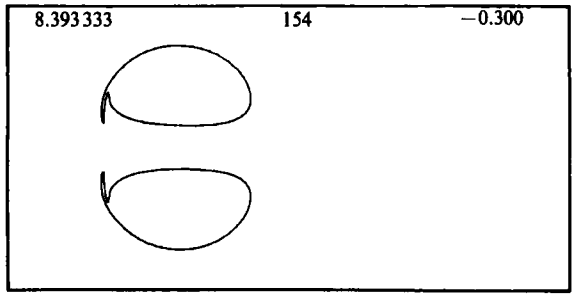

FIGURE 10. Evolution of the vortex with an oblate perturbation of initial amplitude $\epsilon = -0.300$: (*a*) $t^* = 0$; (*b*) 0.213; (*c*) 0.640; (*d*) 1.280; (*e*) 2.560; (*f*) 3.360; (*g*) 4.067; (*h*) 5.153; (*i*) 5.873; (*j*) 7.087; (*k*) 8.393.

9*f–i*); instead, it is convected into the interior of the vortex towards the front stagnation point. In the end of this evolution period (figure 9*i*), the vortex is reduced into a nearly symmetric, steady vortex ring and a secondary toroidal vortex, familiar from the evolution for $\epsilon = -0.050$ (figure 7*i*). The stretching of the secondary vortex discussed previously, becomes clear by comparing figures 9(*i*), (*j*). Simplification of the vortex contour at the stage shown in figure 9(*j*) (causing approximately 2.5% reduction in the flow properties) was necessary for the continuation of the calculations. In the following evolution we observe the formation of a new vortex filament around the front of the vortex ring (figures 9*k*, *l*). This periodic behaviour suggests that as in the $\epsilon = -0.050$ evolution, the flow will tend to an asymptotic state, characterized by the continuous formation of spiral vortex filaments around an almost steady vortex ring.

Behaviour similar to that described above is observed for larger initial amplitudes. As an example, in figure 10, we illustrate the evolution for $\epsilon = -0.300$. In this case, contour simplification resulted in a final 3.5% reduction in the flow properties. Perturbations of still larger initial amplitude deform the vortex in an irregular fashion and thus, they are of limited physical interest.

In summary, we see that the general features of the evolution are in qualitative agreement with linear analysis for both oblate and prolate perturbations. This agreement extends even to finite amplitude perturbations. An important new result of our nonlinear calculations is that in all cases, the flow tends to an asymptotic state. Prolate perturbations lead to a translating vortex core with an elongated vortex tail, while oblate perturbations lead to a vortex ring with an entrained spiral of irrotational fluid. These asymptotic patterns appear to be stable to axisymmetric perturbations, suggesting that azimuthal perturbations are essential for further evolution.

Concluding this section, we would like to discuss the effect of contour simplification ('contour surgery'), on the evolution for oblate perturbations. To address this issue, we performed calculations using different simplification procedures. For instance, we truncated the developed vortex filaments at different stages in the evolution. We found that although the details of the truncation had some effect on the local behaviour around the truncation region, the overall evolution of the vortex remained unchanged. Clearly, thin vortex filaments with bounded vorticity are of minor dynamic significance. Note that Pozrikidis & Higdon (1985) arrived at similar conclusions for two-dimensional vortex flows. Thus, contour simplification is justified as a tool for analysing the main features of the flow dynamics.

5. Discussion

5.1. *A family of steady vortex rings*

In the preceding section we showed that in its asymptotic state, an oblate vortex reduces to a nearly symmetric vortex ring. The properties of this ring, including vortex volume V, circulation C, kinetic energy T and impulse P, must be equal to those of the initial oblate vortex, as these are invariants of vortex motion. Thus, we may characterize an asymptotic ring by the non-dimensional impulse or energy of the initial oblate vortex, $P^* = P/\rho\lambda a^5$, $T^* = T/\rho\lambda^2 a^7$, where a and λ are defined implicitly in terms of the volume $V = \frac{4}{3}\pi a^3$ and the circulation $C = \lambda V$. Under this non-dimensionalization, P^* and T^* are functions of the perturbation parameter ϵ, and the asymptotic rings may be identified by any of the parameters ϵ, P^* and T^*.

Because the asymptotic rings arising from oblate vortices are almost steady, it is of interest to compare them to steady vortex rings described by previous authors. Norbury (1973) developed a numerical method for calculating steady vortex rings with linear vorticity distribution. He described the contour of a ring in the form of a Fourier series

$$\left.\begin{aligned} x &= Lf(t)\sin t, \\ \sigma &= L(1+f(t)\cos t), \end{aligned}\right\} \tag{22}$$

where

$$f(t) = \sum_0^\infty a_n(\alpha)\cos nt, \tag{23}$$

L is the mean vortex radius, and α is a non-dimensional parameter expressing the ring area over a cross-section, $A = \pi L^2\alpha^2$. When $\alpha \to \sqrt{2}$ the ring becomes Hill's spherical vortex, while when $\alpha \to 0$ it becomes a line ring of very small, nearly circular cross-section. It is convenient to scale the properties of Norbury's rings using the above non-dimensionalization (i.e. keeping vortex volume and circulation constant). In this fashion, we may identify a steady ring by any of the parameters α, P^* and T^*.

To compare Norbury's steady rings to the asymptotic rings arising from oblate vortices, we plot the kinetic energy T^* as a function of the impulse P^* for both cases (figure 11) (the energy of the asymptotic rings was evaluated as a contour integral as explained in the Appendix). The circled points in figure 11 show the energy and impulse of steady rings, as given in table 2 by Norbury (1973). It is clear that these points lie below the dashed line for the unsteady oblate vortices. However, this is not allowed by energetic considerations; Benjamin (1975) showed that for given volume, circulation and impulse, an axisymmetric vortex with linear vorticity distribution has maximum energy when it is steady.† Given the accuracy of the curve for oblate vortices, we conclude that the impulse-energy data of Norbury is not accurate enough for our purposes. To obtain a better approximation of the $T^*(P^*)$ curve for steady rings, we use the relationship $\mathrm{d}T^*/\mathrm{d}P^* = W^*$ (Norbury 1973), where W^* is the non-dimensional vortex speed, $W^* = W/\lambda a^2$, and the differential is taken at constant volume and circulation, i.e. at constant a and λ. Integrating this equation, using the data for W^* provided with sufficient accuracy by Norbury, yields the solid curve in figure 11 which correctly lies above and very close to the curve for oblate vortices. Several points on the $T^*(P^*)$ curves for oblate vortices and vortex rings are given in table 1. The fact that the two curves are very close to each other indicates that the development of a nearly steady vortex ring from an oblate vortex is possible

† This theorem includes vortex rings extending to the axis of symmetry, i.e. perturbed Hill's vortices.

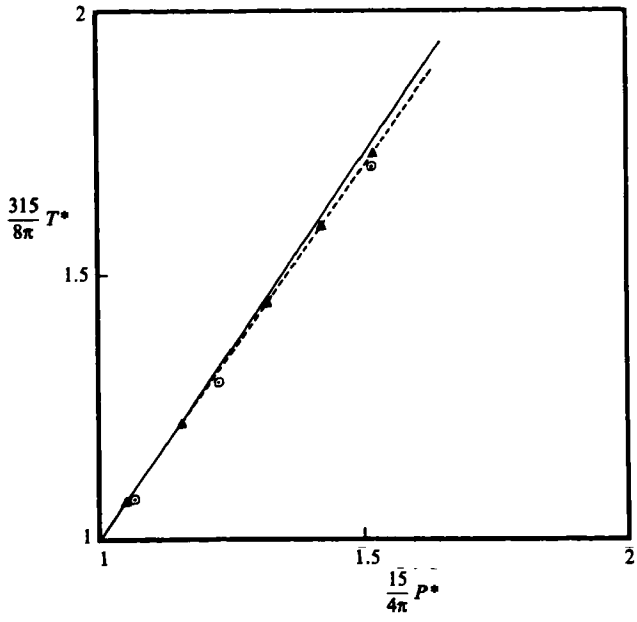

FIGURE 11. Non-dimensional kinetic energy $T^* = T/\rho\lambda^2 a^7$, as a function of the impulse $P^* = P/\rho\lambda a^5$, for prolate vortices (dashed line) and steady rings (solid line). The circled points indicate approximate values for steady rings given in table 2 of Norbury (1973).

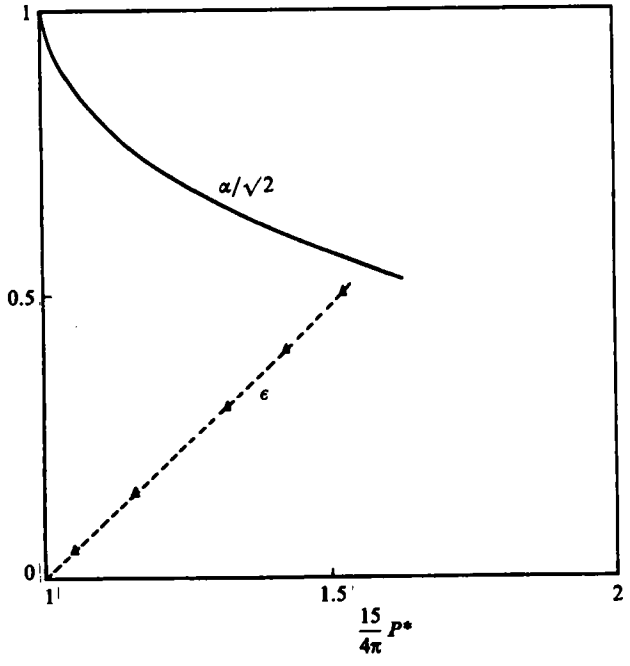

FIGURE 12. Shape parameter α for steady vortex rings, and perturbation parameter ϵ for oblate vortices as functions of the fluid impulse P^*.

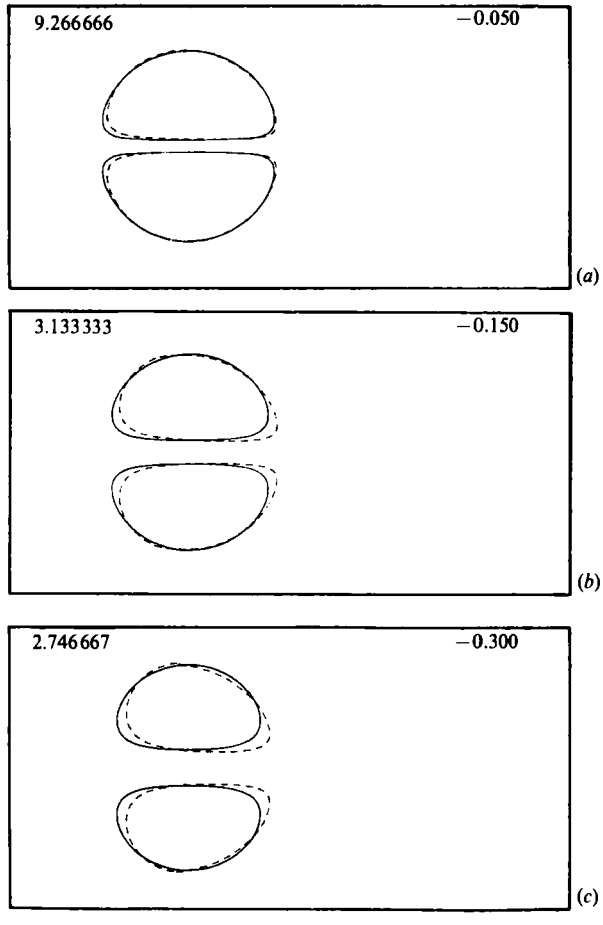

FIGURE 13. Steady vortex rings (solid contours) of impulse and energy approximately the same as those for asymptotic rings (dashed contours) arising from oblate vortices: (a) $\epsilon = -0.050$, $t^* = 9.267$; (b) $\epsilon = -0.150$, $t^* = 3.133$; (c) $\epsilon = -0.300$, $t^* = 2.747$.

		$(315/8\pi)\,T^*$	
$(15/4\pi)\,P^*$	ϵ	Oblate vortices	Steady rings
1.0	0.0	1.0	1.0
1.051	−0.050	1.072	1.072
1.157	−0.150	1.219	1.223
1.320	−0.300	1.448	1.459
1.425	−0.400	1.593	1.612
1.524	−0.500	1.731	1.757

TABLE 1. Impulse P^*, and energy T^* data for oblate vortices and steady vortex rings.

within the constraints imposed by flow invariants. To establish a correspondence between the initial oblate vortices and the steady rings, we plot the parameters α and ϵ, as functions of P^*, figure 12. This yields a unique relationship between α and ϵ. As an example, in figure 13 (solid lines) we present three steady vortex rings with values of α corresponding to $\epsilon = -0.050$, -0.150 and -0.300. Superimposed on these

rings are the asymptotic rings arising from the corresponding oblate perturbations (dashed lines). One can see that the asymptotic rings may be considered as perturbed states of the steady rings, in agreement with our previous observations.

5.2. *Translation of the vortex*

In the previous sections we discussed the evolution of disturbances on Hill's vortex, considering primarily the qualitative features of the motion. In this section we examine how the growth of the perturbation affects the speed of the vortex. It is convenient to specify the position of the vortex using the vorticity centroid (x_c, σ_c), defined by the equations (Lamb 1932 art. 162),

$$\sigma_c^2 = \frac{\int \omega\sigma^2 \,\mathrm{d}\sigma\,\mathrm{d}x}{\int \omega \,\mathrm{d}\sigma\,\mathrm{d}x} = \frac{P}{\pi\rho C}, \tag{24}$$

$$x_c = \frac{\int \omega\sigma^2 x \,\mathrm{d}\sigma\,\mathrm{d}x}{\int \omega\sigma^2 \,\mathrm{d}\sigma\,\mathrm{d}x} = \frac{\pi\rho}{P}\int \omega\sigma^2 x \,\mathrm{d}\sigma\,\mathrm{d}x, \tag{25}$$

where $P = \pi\rho\int\omega\sigma^2\,\mathrm{d}A$ and $C = \int\omega\,\mathrm{d}A$ are the fluid impulse and circulation, both invariants of the motion. Thus, σ_c remains constant, while x_c changes during the motion. Assuming a linear vorticity distribution $\omega = \lambda\sigma$, we may express C, P and x_c as contour integrals,

$$C = -\lambda\pi\oint_{C_v} \sigma^2\,\hat{\boldsymbol{i}}\cdot\hat{\boldsymbol{t}}\,\mathrm{d}l,$$

$$P = \pi\rho\lambda\oint_{C_v} \sigma^3 x\,\hat{\boldsymbol{j}}\cdot\hat{\boldsymbol{t}}\,\mathrm{d}l,$$

$$x_c = \pi\rho\lambda\oint_{C_v} \sigma^3 x^2\,\hat{\boldsymbol{j}}\cdot\hat{\boldsymbol{t}}\,\mathrm{d}l/2P,$$

where $\hat{\boldsymbol{t}}$ and $\hat{\boldsymbol{j}}$ are the unit vectors in the x- and σ-directions. The vortex speed may be expressed as $U_c = \mathrm{d}x_c/\mathrm{d}t$, and can be evaluated as a contour integral in the form

$$U_c = \frac{\pi\rho\lambda}{P}\oint_{C_v} \sigma^3 x\,\boldsymbol{u}\cdot\hat{\boldsymbol{n}}\,\mathrm{d}l,$$

where $\hat{\boldsymbol{n}}$ is the unit normal vector to the contour, pointing out of the vortex.

Figure 14 illustrates the behaviour of the non-dimensional vorticity centroid $x_c^* = x_c/a$ and the vortex speed $U_c^* = \mathrm{d}x_c^*/\mathrm{d}t^*$ for prolate perturbations of different initial amplitude, in a frame of reference which moves with the unperturbed vortex speed U. As the vortex tail develops and vorticity detrains from the core, the vortex moves downstream at an increasing rate. In a stationary frame of reference, this would imply a deceleration of the translating vortex. Note however the short initial period of upstream translation for the small amplitude perturbation, $\epsilon = 0.050$. At large times, as the flow tends to an asymptotic state, the vortex speed tends to an asymptotic value which is closely predicted by linear analysis to be equal to $\frac{2}{5}\epsilon U$. Asymptotic vortex speeds as predicted by linear analysis and numerical calculations are compared in table 2. We conclude that prolate perturbations initiate a slow translation of a steady vortex, or equivalently, a deceleration of a translating vortex.

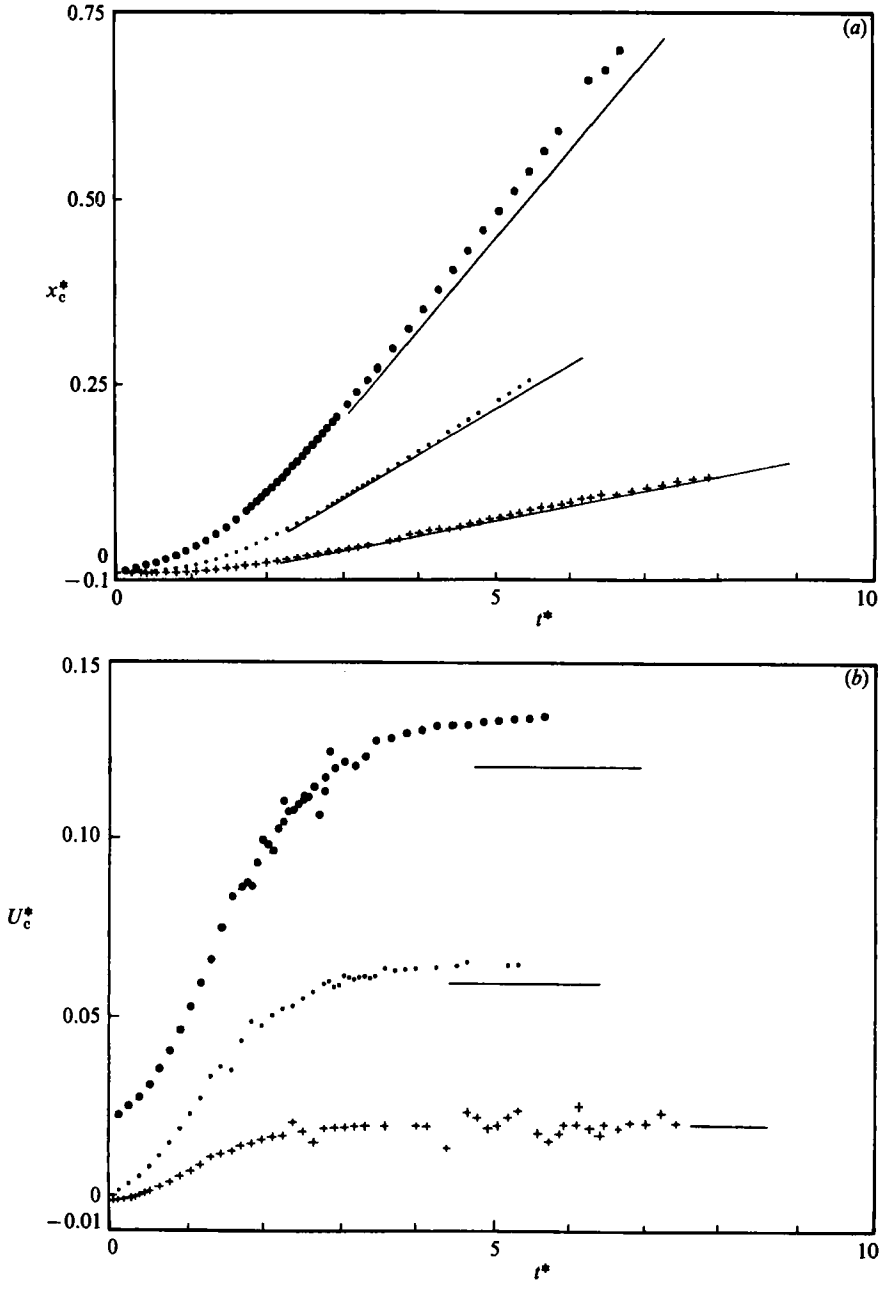

FIGURE 14. Evolution of (*a*) the vorticity centroid $x_c^* = x_c/a$ and (*b*) the vortex speed $U_c^* = \mathrm{d}x_c^*/\mathrm{d}t^*$ for prolate perturbations. The straight lines show predictions of linear analysis: +, $\epsilon = 0.050$; ., 0.150; ●, 0.300.

Proceeding, we examing the behaviour of the vorticity centroid for oblate perturbations, illustrated in figures 15 and 16. The discontinuities in the curves for x_c^* in figure 15 indicate contour simplifications. Note that although these simplifications affect the position of the centroid x_c^*, they have little effect on the behaviour of the vortex speed U_c^*, figure 16. This again indicates that contour simplification does not alter the nature of the evolution. Figure 15 shows that initially, owing to the

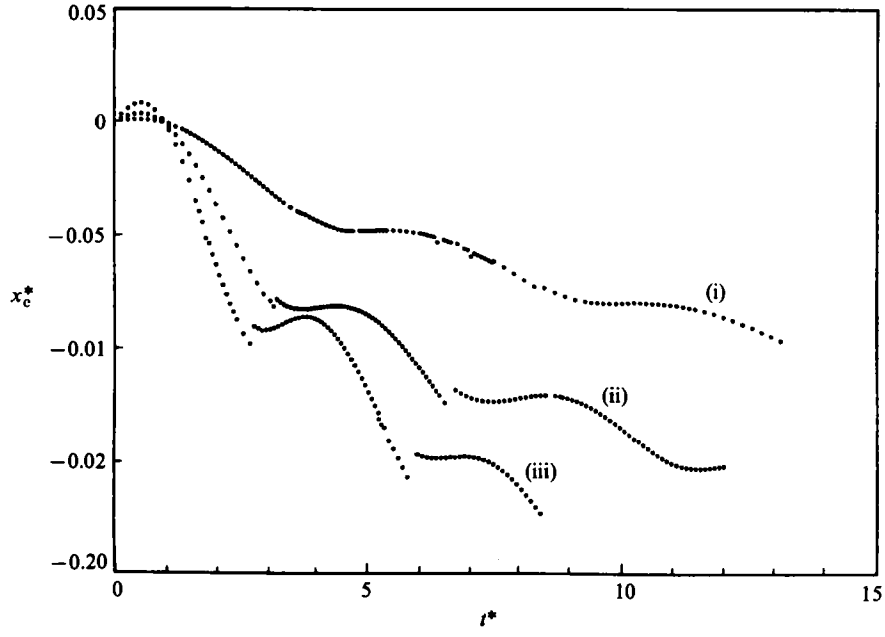

FIGURE 15. Evolution of the vorticity centroid x_c^* for oblate perturbations. The discontinuities indicate contour simplification: (i) $\epsilon = -0.050$; (ii) -0.150; (iii) -0.300.

	U_c^*	
ϵ	Linear theory	Numerical results
0.050	0.020	0.020
0.150	0.060	0.065
0.300	0.120	0.134

TABLE 2. Asymptotic vortex speed U_c^* for prolate perturbations as predicted by linear theory and numerical calculations.

perturbation, the vortex starts translating downstream, at a decreasing rate. In this initial period, U_c^* is positive (figure 16). However, as irrotational fluid is entrained into the vortex causing an expansion, the vortex starts translating upstream at an increasing speed, and U_c^* becomes negative. A maximum negative speed is attained approximately as the entrained fluid reaches the front of the vortex. This is a function of ϵ and is in close agreement with linear predictions for the small perturbations $\epsilon = -0.050$ and -0.150, $U_c^* = \frac{2}{5}\epsilon U$ (figure 16). Interesting behaviour arises thereafter; as the entrained irrotational fluid starts rotating along the vortex boundary, the vortex speed increases and finally, becomes positive. Thus, the generation of a vortex filament is accompanied with an oscillation in the vortex speed. At later times, we find that this oscillation is repeated, owing to the formation of successive vortex filaments around the vortex ring. It is worth noting that the mean value of the oscillations is close to the speed of the corresponding steady vortex rings, Norbury (1973). It should be stressed that this oscillatory behaviour is for a frame of reference translating with the unperturbed vortex speed U. In a stationary frame of reference, the oscillations yield small fluctuations in the vortex speed, or the order 5 %.

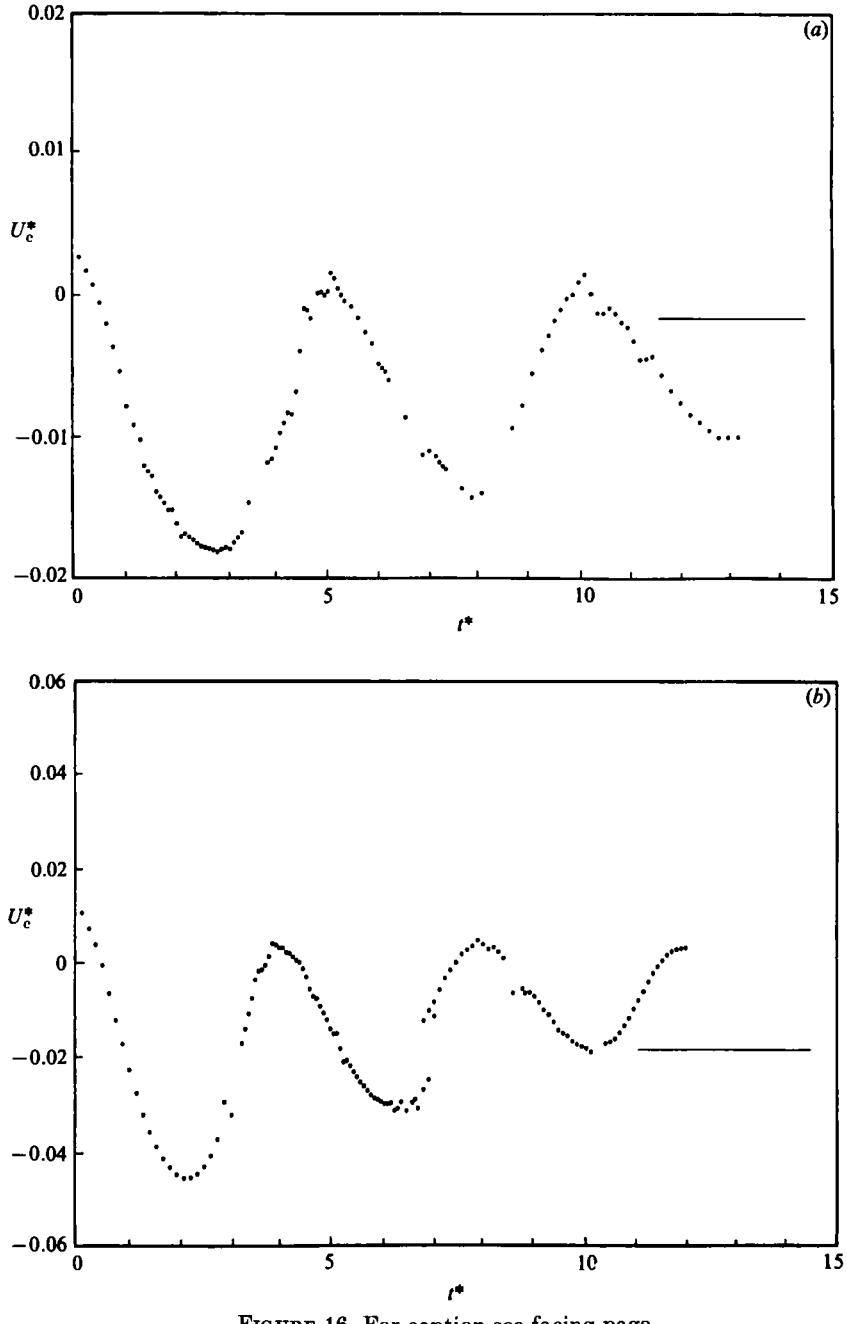

FIGURE 16. For caption see facing page.

6. Concluding remarks

Our calculations indicate the spontaneous development of thin filaments of rotational fluid which appear to demonstrate a singular behaviour. Specifically, they appear to come in contact with each other or with other vortex regions (figures 7*e*, *i*, 9*e*, *j* and 10*e*, *h*, *i*), and to break, separating from the original vortex (figure 5). Most probably, this behaviour is a numerical artifact (owing to the discrete numerical

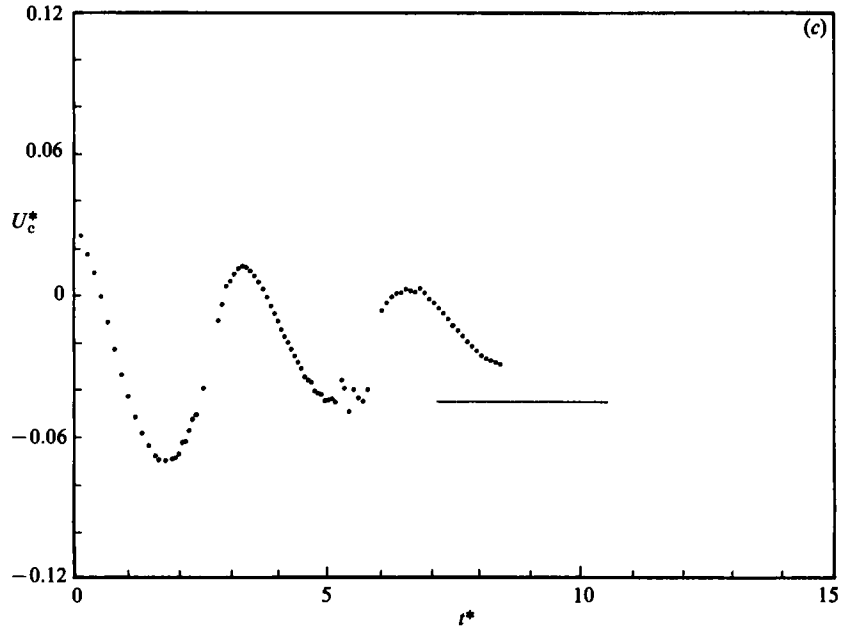

FIGURE 16. Evolution of the vortex speed U_c^* for oblate perturbations. The lower limit of the y-axis corresponds to predictions of linear theory. The horizontal lines show the vortex speed of the corresponding steady vortex rings: (*a*) $\epsilon = -0.050$; (*b*) -0.150; (*c*) -0.300.

representation), which does not affect the global evolution; the appearance of a singularity on a thin vortex filament with bounded vorticity is probably dynamically unimportant. Note that similar behaviour is known to occur in two-dimensional vortex flows, as suggested by the calculations of Overman & Zabusky 1982, and Pozrikidis & Higdon 1985. In the two-dimensional case, the classical results on global existence to the Euler equations show rigorously that two Lagrangian points cannot come together in a finite time and thus, vortex filaments cannot touch or break. It seems likely that similar principles apply for axisymmetric flows, although a theoretical analysis is in order.

The literature contains a large number of experimental studies on the evolution of vortex rings (Maxworthy 1972, 1974, 1977). These rings are usually produced in the laboratory by impulsively pushing a fluid through an orifice or a piston and thus, they are generated by means of roll-up of vortex sheets. The vorticity distribution inside these rings is not linear, but shows a distinct peak along a well-defined vortex core. Furthermore, the evolution of these rings is dominated by viscous effects and three-dimensional instabilities. Thus, unfortunately, a comparison between these studies and our results is not appropriate.

In conclusion, we would like to stress that the contour dynamics formulation, developed in §2, offers an efficient method for analysing a variety of important flows at high Reynolds number. Calculation of steady wakes behind axisymmetric objects (Saffman 1981; Saffman & Tanveer 1984), and analysis of the interaction of vortex rings of finite cross-section (Yamada & Matsui 1977), constitute two interesting applications. An extension of the method to account for periodic flows will provide a useful tool for studying the nonlinear instability of circular jets.

I would like to thank Professor J. J. L. Higdon for his support during the course of this work. This work was supported by the NSF under grant MEA 83-51649.

Appendix

In this appendix we derive an expression for the kinetic energy T of the flow induced by a closed, axisymmetric vortex with linear vorticity distribution $\omega = \lambda\sigma$, as an integral over the vortex contour. First, following Batchelor (1967 §7.2), we write

$$T = \tfrac{1}{2}\rho \int (u^2+v^2)\,\mathrm{d}V = \pi\rho \int_{A_\mathrm{v}} \omega\psi\,\mathrm{d}\sigma\,\mathrm{d}x = \pi\rho\lambda \int_{A_\mathrm{v}} \psi\sigma\,\mathrm{d}\sigma\,\mathrm{d}x, \tag{A 1}$$

where A_v is the cross-section of the vortex on a semi-infinite plane bounded by the axis of symmetry. To convert the area into a line integral we use Green's theorem

$$\int_{A_\mathrm{v}} [\psi\nabla^2 f - f\nabla^2\psi]\,\mathrm{d}\sigma\,\mathrm{d}x = \int_{C_\mathrm{v}} [\psi\nabla f - f\nabla\psi]\cdot\hat{\boldsymbol{n}}\,\mathrm{d}l, \tag{A 2}$$

where f is a twice differentiable function, $\nabla^2 = \partial^2/\partial x^2 + \partial^2/\partial\sigma^2$, C_v denotes the vortex contour and $\hat{\boldsymbol{n}}$ is the unit normal to C_v pointing out of the vortex. Choosing $f = \frac{1}{6}\sigma^3$ and recalling that $\nabla^2\psi = -\omega\sigma + (\partial\psi/\partial\sigma)/\sigma$ (equation (2)), we substitute into (A 2), integrate by parts in the left-hand side and use the divergence theorem to write

$$T = \tfrac{3}{4}\pi\rho\lambda \int_{C_\mathrm{v}} \left[\left(\tfrac{2}{3}\psi - \frac{\lambda}{36}\sigma^4\right)\hat{\boldsymbol{j}}\cdot\hat{\boldsymbol{n}} + \tfrac{1}{6}\sigma^2\boldsymbol{u}\cdot\hat{\boldsymbol{t}}\right]\sigma^2\,\mathrm{d}l. \tag{A 3}$$

In this expression, $\hat{\boldsymbol{t}}$ is the unit tangent to C_v, $\hat{\boldsymbol{j}}$ is the unit vector in the radial direction and the integral is evaluated in the counterclockwise sense.

Note that the stream function may be evaluated from the velocity using the relationship

$$\psi(\boldsymbol{x}) = \psi(\boldsymbol{x}_0) + \int_{\boldsymbol{x}_0}^{\boldsymbol{x}} \sigma\,\boldsymbol{u}\cdot\hat{\boldsymbol{n}}\,\mathrm{d}l, \tag{A 4}$$

with reference value $\psi = 0$ along the axis of symmetry, and the velocity may be evaluated as a contour integral, as explained in §2.

REFERENCES

Abramowitz, M. & Stegun, I. 1972 *Handbook of Mathematical Functions*. Dover.

Batchelor, G. K. 1967 *An Introduction to Fluid Dynamics*. Cambridge University Press.

Benjamin, T. B. 1975 The alliance of practical and analytical insights into the nonlinear problems of fluid mechanics. *Lect. Notes Maths* **503**, 9–29.

Bliss, D. B. 1973 The dynamics of flows with high concentrations of vorticity. Ph.D. thesis, Dept. of Aer. and Astr. M.I.T.

Davis, H. T. 1960 *Introduction to Nonlinear Differential and Integral Equations*. Dover.

Deem, S. G. & Zabusky, N. J. 1978 Vortex waves: stationary 'V states', interactions, recurrence and breaking. *Phys. Rev. Lett.* **40**, 859–862.

Durst, F. & Schönung, B. 1982 Computations of steady, ellipsoidal vortex rings with finite cores. *Comp. Fluids*, **10** (1), 87–93.

Harper, J. F. & Moore, D. W. 1968 The motion of a spherical liquid drop at high Reynolds numbers. *J. Fluid Mech.* **32**, 367–391.

Hill, M. J. M. 1894 On a spherical vortex. *Phil. Trans. R. Soc. Lond.* A **185**, 213–245.

Lamb, H. 1932 *Hydrodynamics*. Dover.

MAXWORTHY, T. 1972 The structure and stability of vortex rings. *J. Fluid Mech.* **51**, 415–432.

MAXWORTHY, T. 1974 Turbulent vortex rings. *J. Fluid Mech.* **64**, 227–239.

MAXWORTHY, T. 1977 Some experimental studies of vortex rings. *J. Fluid Mech.* **81**, 465–495.

MOFFATT, H. K. & MOORE, D. W. 1978 The response of Hill's spherical vortex to a small axisymmetric disturbance. *J. Fluid Mech.* **87**, 749–760.

MOORE, D. W. 1962 The boundary layer on a spherical gas bubble. *J. Fluid Mech.* **16**, 161–176.

NORBURY, J. 1973 A family of steady vortex rings. *J. Fluid Mech.* **57**, 417–431.

O'BRIEN, V. 1961 Steady spheroidal vortices – more exact solutions to the Navier–Stokes equation. *Q. Appl. Maths* **19**, 163–168.

OVERMAN, A. E. & ZABUSKY, N. J. 1982 Evolution and merger of isolated structures. *Phys. Fluids.* **25** (8), 1297–1305.

PIERREHUMBERT, R. T. & WIDNALL, S. E. 1981 The structure of organized vortices in a free shear layer. *J. Fluid Mech.* **102**, 301–313.

POZRIKIDIS, C. & HIGDON, J. J. L. 1985 Nonlinear Kelvin–Helmholtz instability of a finite vortex layer. *J. Fluid Mech.* **157**, 225–263.

SAFFMAN, P. G. 1981 Dynamics of vorticity. *J. Fluid Mech.* **106**, 49–58.

SAFFMAN, P. G. & SZETO, R. 1981 Structure of a linear array of uniform vortices. *Stud. Appl. Maths* **65**, 223–248.

SAFFMAN, P. G. & TANVEER, S. 1984 Prandtl–Batchelor flow past a flat plate with a forward-facing flap. *J. Fluid Mech.* **143**, 351–365.

TURNER, J. S. 1964 The flow into an expanding spherical vortex. *J. Fluid Mech.* **18**, 195–209.

WEGENER, P. P. & PARLANGE, J. Y. 1973 Spherical-cap bubbles. *Ann. Rev. Fluid Mech.* **11**, 79–100.

YAMADA, H. & MATSUI, T. 1977 Preliminary study of mutual slip-through of a pair of vortices. *Phys. Fluids* **21** (2), 292–294.